JOURNAL OF AIRCRAFT
Vol. 47, No. 4, July–August 2010

Flight Test of Stable Automated Cruise Flap for an Adaptive Wing Aircraft

Craig Cox,* Ashok Gopalarathnam,† and Charles E. Hall Jr.†
North Carolina State University, Raleigh, North Carolina 27695

DOI: 10.2514/1.46789

Cruise flaps are trailing-edge flaps that are adjusted to minimize drag by moving the location of the low-drag region of an airfoil drag polar to match the current coefficient of lift. Previous research explored the use of a wing-based pressure-differential ratio called $\Delta C_p'$ to automate cruise flaps. Rigid-aircraft simulations showed the effectiveness of a controller implementing multiple functions using $\Delta C_p'$. The gust-alleviation function reduced coefficient-of-lift perturbations, the $\Delta C_p'$-optimization function reduced drag, and the $\Delta C_p'$-maintenance function maintained the current trim $\Delta C_p'$ in the presence of pilot elevator inputs. In this research, the $\Delta C_p'$-optimization and $\Delta C_p'$-maintenance functions were implemented using low-cost microcontrollers and pressure transducers. Flight tests were performed using a radio-controlled sailplane with a wing span of 100 inches. Although direct measurement of drag for aircraft of this size is difficult and was not attempted, analysis of the data showed that the $\Delta C_p'$-optimization function was effective in producing pressure differentials that would have reduced drag. The effectiveness of the $\Delta C_p'$-maintenance function could not be determined because of large sample-to-sample variations in measured $\Delta C_p'$ values. It remains unknown whether this high-frequency content actually represented rapidly varying pressures on the airfoil surface or if it was the result of noise in the measurement system.

Nomenclature

C_L	=	aircraft lift coefficient
C_d	=	airfoil drag coefficient
C_l	=	airfoil lift coefficient
$G_C(s)$	=	transfer function for the proportional–integral–derivative or proportional–integral controller that implements pressure-differential optimization
$G_F(s)$	=	transfer function for the low-pass filter that processes pressure-differential error
K_I	=	integral gain
K_P	=	proportional gain
p_l	=	midchord lower-surface pressure
$p_{l,l}$	=	leading-edge lower-surface pressure
$p_{l,u}$	=	leading-edge upper-surface pressure
p_u	=	midchord upper-surface pressure
s	=	variable used in the Laplace transform representation of control system transfer functions
$\Delta C_p'$	=	ratio of leading-edge pressure differential to absolute value of midchord pressure differential
δ_e	=	elevator deflection angle
$\delta_{e,c}$	=	commanded elevator deflection angle
δ_f	=	flap deflection angle

Introduction

CRUISE flaps are trailing-edge flaps operated at small deflection angles for the purpose of reducing drag at offdesign conditions. The deflection of a cruise flap results in a shifting of the low-drag region (LDR) of the drag polar for an airfoil, as shown in Fig. 1. Flap deflection moves the leading-edge stagnation point, which affects the pressure distributions along the airfoil upper and lower surfaces. Figure 2 shows that for natural laminar flow (NLF) airfoils, there is a small region at the leading edge where it is most desirable to locate the stagnation point [1,2]. Doing so results in favorable (or less adverse) pressure gradients over the upper and lower surfaces, even at offdesign coefficients of lift. Without the cruise flap, either the upper or lower surface would experience loss of laminar flow at these offdesign conditions. Thus, when scheduled correctly, a cruise flap can result in a large range of C_l values over which low C_d is achieved. For this reason, several NLF airfoils have been designed with cruise flaps [3–5]. Cruise flaps have also been successfully used on high-performance sailplanes for several decades.

A study of automated cruise flaps was performed by McAvoy and Gopalarathnam [6]. The four pressure sensors shown in Fig. 3 were used to determine the pressure differentials between top and bottom surfaces near the leading-edge and midchord locations. Comparing the leading-edge differential with the midchord differential results in a scalar defined by the following equation:

$$\Delta C_p' = \frac{p_{l,u} - p_{l,l}}{|p_u - p_l|}$$

A number of NLF airfoils were examined by plotting $\Delta C_p'$ against lift coefficient for different flap angles. Figure 4 shows the results for an NLF airfoil designed for a hypothetical unmanned aerial vehicle. For each flap deflection, locations corresponding to the upper and lower corners of the low-drag region are marked with hollow and solid circles, respectively. For this airfoil, a target $\Delta C_p'$ value of -1.0 ensures operation in the low-drag region regardless of lift coefficient or flap deflection angle. McAvoy and Gopalarathnam [6] proposed a controller that would move the flap to maintain a constant $\Delta C_p'$ value of -1.0 and showed the drag reduction that would occur as a result of such an automated cruise flap.

Vosburg and Gopalarathnam [7] noted that an automated cruise flap could be controlled using the instantaneous coefficient of lift as the sole input. Such a flap, however, would be unstable by itself. From a trimmed state, if the wing was perturbed such that the coefficient of lift was increased, the flap angle would increase to move the stagnation point back to the ideal location. The larger flap angle would then increase the coefficient of lift even more, and the flap would quickly diverge to its limit of travel. Although aircraft

Presented as Paper 2009-5728 at the AIAA Guidance, Navigation and Control Conference, Chicago, IL, 10–13 August 2009; received 25 August 2009; revision received 2 November 2009; accepted for publication 3 November 2009.

*Graduate Research Assistant, Department of Mechanical and Aerospace Engineering; currently Aerospace Engineer, Aerodynamic Configuration Branch, U.S. Air Force Research Laboratory, 2130 Eighth Street, Wright-Patterson AFB, OH 45433. Member AIAA.

†Associate Professor, Department of Mechanical and Aerospace Engineering, Campus Box 7910. Senior Member AIAA.

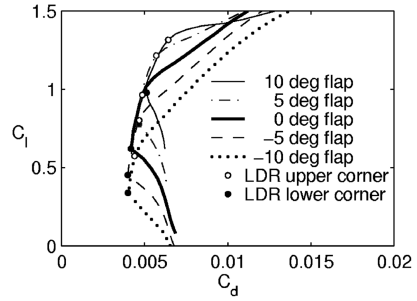

Fig. 1 Shift of low-drag region with flap deflection.

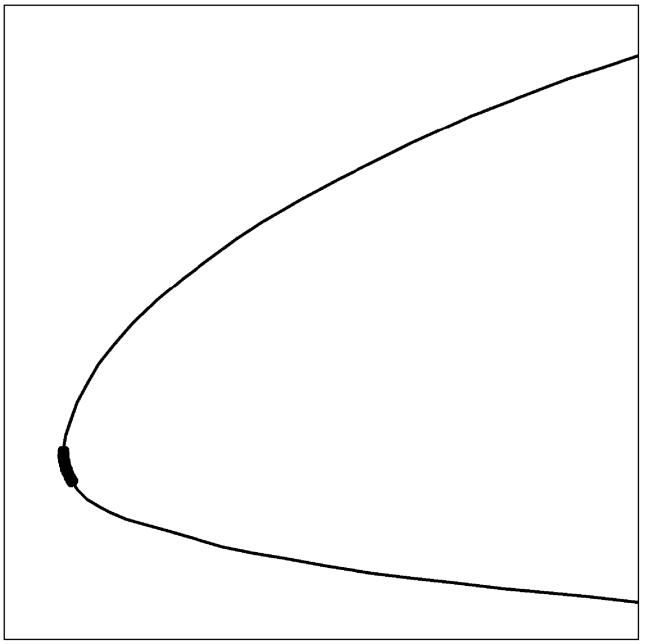

Fig. 2 Ideal stagnation-point range.

such as uninhabited air vehicles are probably equipped with separate autopilot control systems to maintain altitude and airspeed, such systems would not counter the instability of the flap controller, since the flap system has such a short time constant (determined primarily by the reaction time of the flap servo). A filter is needed to slow the operation of the flap.

Cox et al. [8] performed a dynamic stability analysis of the Vosburg and Gopalarathnam [7] controller to show its behavior under different operating conditions and with different filters. They also developed an aircraft controller to maintain a desired coefficient of lift using flap deflections. This type of controller would be useful with segmented flaps for tailoring the spanwise lift distribution to minimize induced drag or wing-root bending moment.

In a follow-on effort, Cox et al. [9] developed an automated cruise flap controller with multiple functions and performed simulations to demonstrate its effectiveness. The aircraft used for the simulations was the Spirit 100 sailplane [10]; Table 1 contains specifications for this aircraft. The Spirit 100 was chosen because it has a fairly large wingspan (100 in.) and was readily available for use in later flight tests. Although limited wind-tunnel testing of the controller could have been performed, the available tunnel could not generate pitch

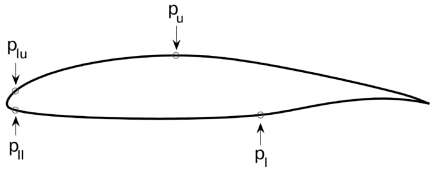

Fig. 3 Pressure-port locations.

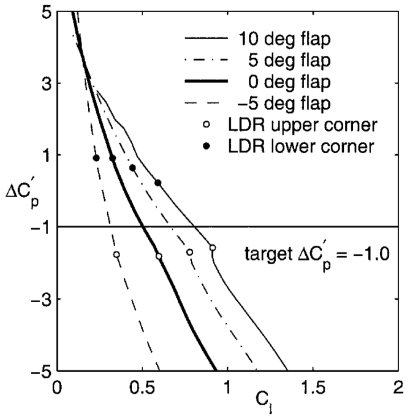

Fig. 4 Plot of $\Delta C_p'$ against C_l showing a target $\Delta C_p'$ value of −1.0, which ensures operation in the low-drag region.

rates achievable by a free-flying aircraft, and so flight tests were deemed essential.

Stability derivatives for the Spirit 100 were determined using the aircraft configuration analysis code AVL [11]. Figure 5 shows the vortex-lattice model that was used as the input to AVL. The SD7037 airfoil used on the Spirit 100 was analyzed using the airfoil analysis code XFOIL [12]. For this airfoil, −1.85 was determined to be the target $\Delta C_p'$ value that would reduce drag over a reasonable range of lift coefficients. Pressure distributions on the airfoil upper and lower surfaces were examined to determine the relationships between flap deflection angle, coefficient of lift, and $\Delta C_p'$. Combining these relationships with aircraft stability derivatives allowed the determination of new coefficients necessary to implement the controller. One example of a newly derived coefficient was the amount of elevator required to change the aircraft lift coefficient by 1.0 if the flap was simultaneously actuated to keep $\Delta C_p'$ constant.

The automated cruise flap controller implemented three different functions. The fast-acting gust-alleviation function reduced perturbations in lift coefficient due to vertical gusts. The slow-acting $\Delta C_p'$-optimization function reduced wing profile drag by adjusting the location of the airfoil low-drag region to match the current coefficient of lift. This was accomplished by driving $\Delta C_p'$ to the target value of −1.85. The fast-acting $\Delta C_p'$-maintenance function responded to elevator inputs from the pilot in a manner such that the desired aircraft response was obtained but the steady-state $\Delta C_p'$ did not change.

The effectiveness of the $\Delta C_p'$-optimization function is shown in Fig. 6. In this simulation, the Spirit 100 was trimmed for an airspeed of 7.8 m/s and was subject to random, rapidly varying, vertical gusts. The trim elevator angle for this airspeed was −1.9 deg, and there was no flap deflection. At this airspeed and flap angle, the open-loop $\Delta C_p'$ was about −2.1. The controller was initially disabled, and although the value of $\Delta C_p'$ varied due to the vertical gusts, its mean value remained approximately −2.1. When the $\Delta C_p'$-optimization function was enabled at 60 s, the flap and elevator began deflecting to

Table 1 Specifications of the Spirit 100 sailplane used for simulations and flight tests

Wing span	2.46 m
Wing area	0.60 m^2
Mean aerodynamic chord	0.25 m
Mass	2.05 kg
Wing loading	3.40 kg/m^2
I_{xx}	0.42 $kg \cdot m^2$
I_{yy}	0.15 $kg \cdot m^2$
I_{zz}	0.56 $kg \cdot m^2$
I_{xz}	0.00 $kg \cdot m^2$
Airspeeds (typical)	7–12 m/s
Reynolds number (nominal)	123,000
Airfoil	SD7037

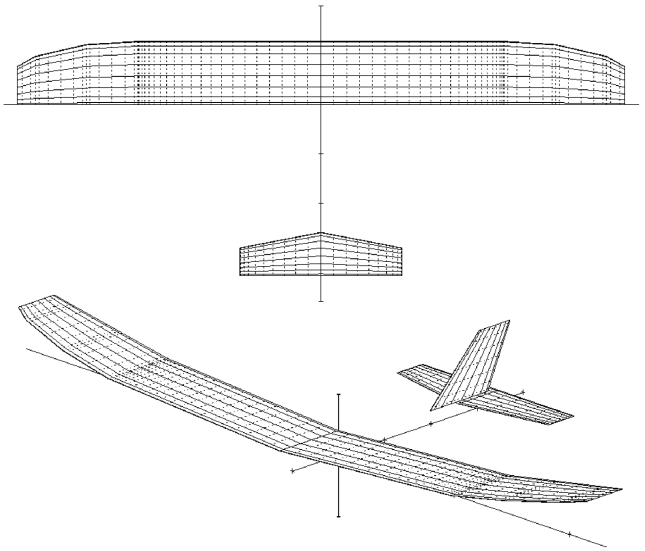

Fig. 5 Vortex-lattice model of a Spirit 100 sailplane.

move $\Delta C'_p$ up to the target value of -1.85. Although not visible in this figure, the mean values of airspeed and lift coefficient were unchanged by the activation of the controller. The amounts of flap and elevator deflection shown were determined using two of the new coefficients derived from the combination of AVL stability derivatives and XFOIL $\Delta C'_p$ data. Specifically, these coefficients were the flap and elevator deflections necessary to generate a desired change in $\Delta C'_p$ while keeping the aircraft lift coefficient constant. This figure shows that the $\Delta C'_p$-optimization function was successful in slowly driving $\Delta C'_p$ to the target value of -1.85.

Figure 7 shows the effectiveness of the $\Delta C'_p$-maintenance function. This simulation started with the same initial conditions as the test of the $\Delta C'_p$-optimization function, except that there were no vertical gusts, and so $\Delta C'_p$ was steady at -2.1. After 10 s the elevator was deflected an additional -1 deg, from -1.9 to -2.9. The value of $\Delta C'_p$ dropped to a mean of about -2.25 and oscillated due to the phugoid response resulting from the change in elevator angle. After about 15 s more, the elevator was returned to the original deflection, and mean $\Delta C'_p$ returned to the original value near -2.1. This portion of the simulation showed that an elevator change commanded by a pilot would result in a change in mean $\Delta C'_p$, which would be undesirable when the $\Delta C'_p$-optimization function was attempting to maintain a constant target $\Delta C'_p$.

At 60 s in Fig. 7 the $\Delta C'_p$-maintenance function was activated, and another elevator pulse was commanded at 70 s. With the controller activated, however, the elevator command was not passed directly to the control surface, but was instead processed by the controller. The controller converted the elevator request into the combination of flap and elevator that would give the same aircraft response as the original elevator request, but would do so without changing trim $\Delta C'_p$. For this aircraft, the -1 deg elevator request was converted into -0.202 deg of elevator and $+2.65$ deg of flap. Although not visible in the figure, this produced the same aircraft lift and airspeed response as the original -1 deg elevator request, but without changing trim $\Delta C'_p$. The figure shows that the mean $\Delta C'_p$ from 70 to 85 s was not affected by the pilot-requested elevator change and resulting aircraft motion, although there were still oscillations due to the phugoid response. The -0.202 deg elevator deflection and $+2.65$ deg flap deflection seen in this simulation were determined using new coefficients obtained from the combination of AVL stability derivatives and XFOIL $\Delta C'_p$ data. This figure shows that the $\Delta C'_p$-maintenance function was successful in maintaining the current steady-state $\Delta C'_p$ even in the presence of elevator inputs from the pilot.

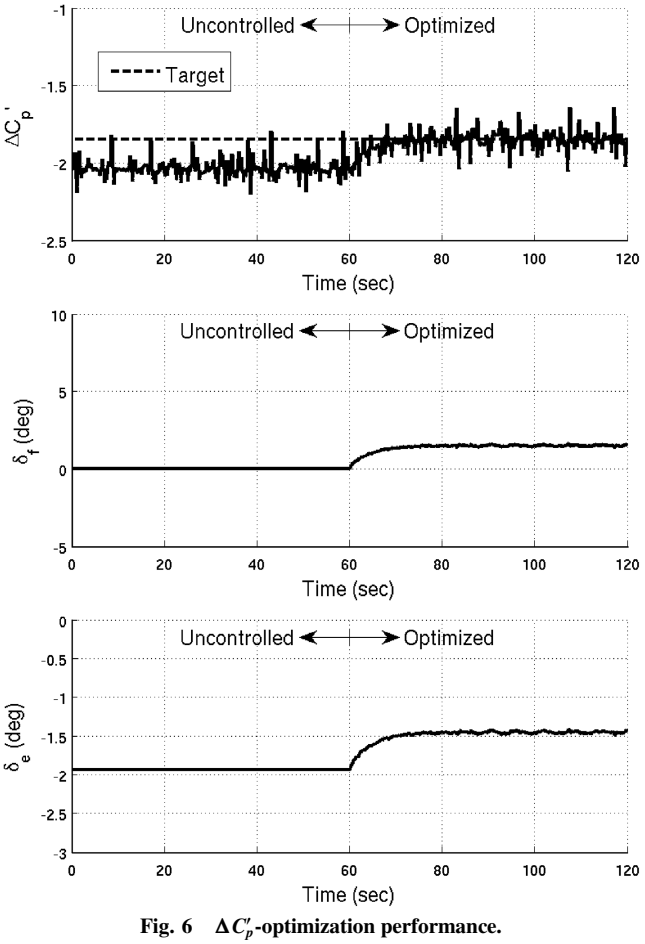

Fig. 6 $\Delta C'_p$-optimization performance.

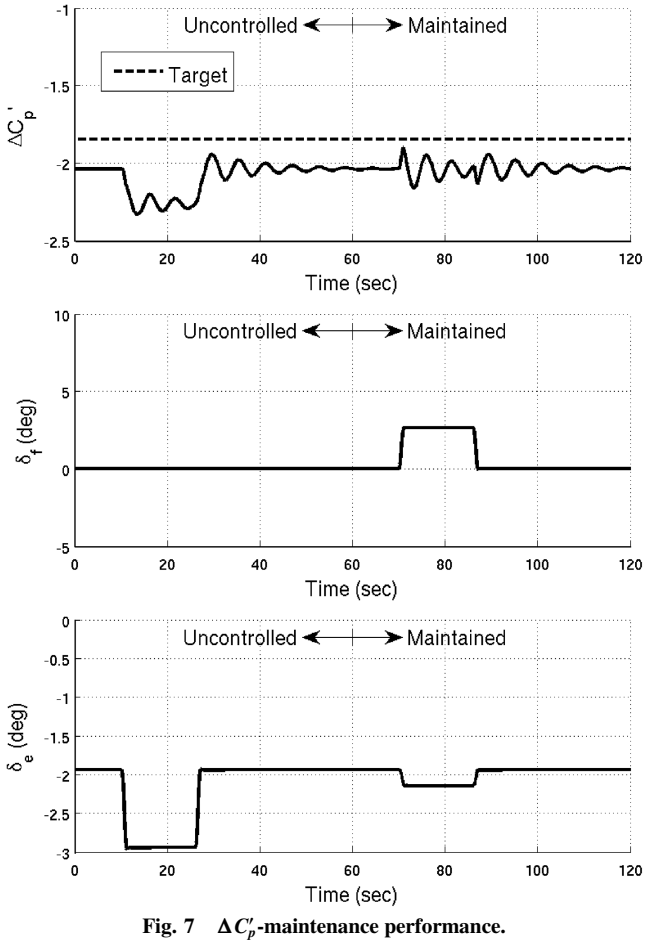

Fig. 7 $\Delta C'_p$-maintenance performance.

Fig. 8 Illustration of the flight-test Spirit 100 sailplane (copyrighted by Great Planes Model Manufacturing Company and used with permission).

Figure 8 is an illustration of the flight-test article used in the current research. More information about the development and flight test of the controller is available in [13].

Controller Hardware/Software

The controller previously used for simulations was modified for the flight-test portion of the research. The gust-alleviation function was not implemented due to limitations of the available hardware. The $\Delta C'_p$-optimization function used in simulation contained a PID (proportional–integral–derivative) block. The contribution of the derivative term was found to be minimal, and so the flight controller used a PI (proportional–integral) block instead of a PID block. The $\Delta C'_p$-maintenance function was implemented identically in simulation and flight test. Figures 9 and 10 are block diagrams of the optimization and maintenance functions implemented for flight testing.

The controller was implemented using 8-bit PIC® microcontrollers from Microchip Technology, Inc. The controller was composed of five different modules. Each module contained a single microcontroller and the software necessary to carry out the task of the module. The five modules were the $\Delta C'_p$ reader, servo reader, servo writer, servo calculator, and fail-safe switch.

The purpose of the $\Delta C'_p$ reader module was to convert pressures from the leading-edge and midchord wing ports to raw $\Delta C'_p$ values. It also subtracted the target $\Delta C'_p$ value of -1.85 from raw values and passed the difference through a low-pass filter with a time constant of 20 s to determine the filtered $\Delta C'_p$ error. It was this filtered $\Delta C'_p$ error that was used in the $\Delta C'_p$-optimization function. The following is the continuous-time transfer function for the low-pass filter:

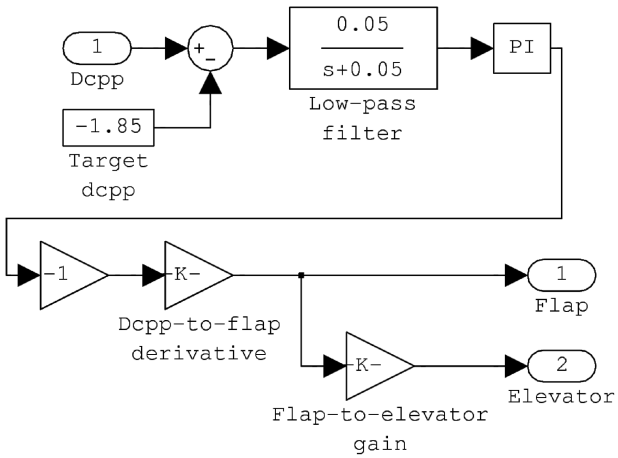

Fig. 9 $\Delta C'_p$-optimization function.

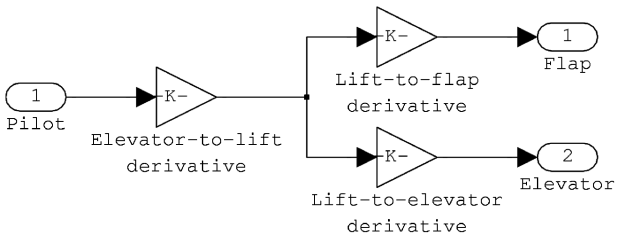

Fig. 10 $\Delta C'_p$-maintenance function.

$$G_F(s) = \frac{0.05}{s + 0.05}$$

The time constant of 20 s was chosen to be much longer than the expected phugoid period of the aircraft (about 6 s). The pressure transducer used for the leading-edge differential had a range of ± 1 in. of water (± 250 Pa); the transducer for the midchord differential had a range of 0–1 in. of water (0–250 Pa). The microcontroller for the $\Delta C'_p$ reader was a PIC12F675 from Microchip Technology, Inc.

The purpose of the servo reader was to monitor signals from the radio-controlled (R/C) receiver and calculate servo positions based on the widths of pulses on the flap, elevator, aileron, and landing-gear servo lines. The Spirit 100 does not have retractable landing gear, and so the gear switch on the transmitter was available for use as a controller-enable switch. Monitoring the gear servo line allowed the controller to know when it should be applying $\Delta C'_p$ maintenance and $\Delta C'_p$ optimization and when it should pass pilot inputs directly to the control surfaces without modification. The microcontroller for the servo reader was a PIC16F630 from Microchip Technology, Inc.

The purpose of the servo writer was to convert servo positions generated by the servo calculator into pulses that were sent to the servos and recorded by the onboard EagleTree data recorder. Flap and aileron signals were mixed in order to implement full-span flaps whenever the controller was enabled. All pulse widths were constrained to ranges that correspond to the manufacturer-recommended control surface throws for the Spirit 100. Raw $\Delta C'_p$ and filtered $\Delta C'_p$ error were converted into servolike pulses that were recorded by EagleTree. The microcontroller for the servo writer was a PIC16F630 from Microchip Technology, Inc.

The servo calculator was the master module that coordinated the functionality of the $\Delta C'_p$ reader, servo reader, and servo writer modules. It ensured that servo signals were updated every 20 ms for an update rate of 50 Hz. It modified flap and elevator commands to implement the $\Delta C'_p$-maintenance and $\Delta C'_p$-optimization functions of the controller.

The $\Delta C'_p$-maintenance function converted pilot elevator requests into combinations of elevator and flap that provided the expected changes in trim aircraft C_L, but without any changes in trim $\Delta C'_p$. For the Spirit 100 sailplane at a trim airspeed of 7.8 m/s, this required that every 1 deg of elevator requested by the pilot be converted into 0.202 deg of elevator and -2.65 deg of flap. These values were determined using a combination of stability derivatives from AVL and $\Delta C'_p$ data from XFOIL. The following is the control law that was implemented for $\Delta C'_p$ maintenance:

$$\delta_e = 0.202\,\delta_{e,c} \qquad \delta_f = -2.65\,\delta_{e,c}$$

The $\Delta C'_p$-optimization function responded to nonzero filtered $\Delta C'_p$ error by actuating flap and elevator in a manner such that trim $\Delta C'_p$ was changed, but not trim wing C_L. This was a two-part process. First, the filtered $\Delta C'_p$ error was passed through a PI control block with the following continuous-time transfer function:

$$G_C(s) = \frac{4s + 0.195}{s}$$

The K_P and K_I values of 4 and 0.195 were determined in the simulation phase of the research by manually tuning the controller to provide a stable response to changes in the input. The output of this PI block was then multiplied by the elevator and flap deflections necessary to correct a unit error of $\Delta C'_p$. For the Spirit 100 at 7.8 m/s, it was determined that -8.95 deg of flap and -2.93 deg of elevator would correct a unit error of $\Delta C'_p$ without changing wing C_L. These values were obtained using AVL stability derivatives and XFOIL $\Delta C'_p$ data. The following (which includes the low-pass filter $G_F(s)$ and PI block $G_C(s)$) is the control law that was implemented for $\Delta C'_p$ optimization. Both control surface deflection angles are in degrees:

$$\delta_f = -1.79\left(\frac{s+0.0488}{s^2+0.05s}\right)(\Delta C'_p + 1.85)$$

$$\delta_e = -0.587\left(\frac{s+0.0488}{s^2+0.05s}\right)(\Delta C'_p + 1.85)$$

The complete control law implemented by the controller was the sum of the laws implemented for $\Delta C'_p$ optimization and $\Delta C'_p$ maintenance:

$$\delta_f = -1.79\left(\frac{s+0.0488}{s^2+0.05s}\right)(\Delta C'_p + 1.85) - 2.65\,\delta_{e,c}$$

$$\delta_e = -0.587\left(\frac{s+0.0488}{s^2+0.05s}\right)(\Delta C'_p + 1.85) + 0.202\,\delta_{e,c}$$

The coefficients in the above equations are products of the low-pass filter time constant, the controller K_P and K_I gains, and the new cruise flap derivatives calculated from AVL stability derivatives and XFOIL $\Delta C'_p$ data. The microcontroller for the servo calculator was a PIC12F629 from Microchip Technology, Inc.

The fail-safe switch monitored the landing-gear servo signal from the R/C receiver. This signal was used by the pilot to determine whether or not the controller was to be enabled. It allowed the pilot to disable the controller if it malfunctioned and to safely terminate the flight. The microcontroller for the fail-safe switch was a PIC12F629 from Microchip Technology, Inc.

Since the five modules of the controller were implemented using separate microcontrollers for each, a challenge/response scheme was developed to allow reliable communications between them. All data messages were digital to prevent analog noise between the modules from affecting transferred data ($\Delta C'_p$ values, servo pulse widths, etc.) Although analysis of the flight data would later reveal that the $\Delta C'_p$ data were very noisy, the design of the digital communications scheme ensured that it did not contribute to any of this noise.

Flight Tests and Analysis

Several flight tests were performed to evaluate the effectiveness of the controller. It was found that raw $\Delta C'_p$ values varied significantly from one recorded sample to the next. The cause of these variations remains unknown. There are at least three possibilities. First, the actual pressures at the ports could have been fluctuating very rapidly due to manufacturing imperfections or other reasons not currently understood. Second, all A/D converters will exhibit some discretization error, and something in the flight environment may have exacerbated the small transducer noise that was observed in a laboratory environment. Third, the $\Delta C'_p$ values were converted to pulse widths that were then measured and recorded by the EagleTree data logger. There may have been noise in the EagleTree subsystem used to measure pulse widths.

Regardless of the reasons for the $\Delta C'_p$ fluctuations, the data were noisy enough that it was not useful to display them directly. The relative size of the fluctuations made it difficult to determine trends in the local mean values. For this reason, $\Delta C'_p$ values were passed through a central moving-average filter with a window size of 1 s (10 samples). A 1 s window smoothed the sample-to-sample fluctuations but still allowed for a determination of how $\Delta C'_p$ was changing second-by-second. In this document, three types of $\Delta C'_p$ are discussed. The set of instantaneous measured $\Delta C'_p$ values is called *raw* $\Delta C'_p$. These raw data are passed through the previously discussed low-pass filter, and the output of this operation is called *filtered* $\Delta C'_p$. It is filtered $\Delta C'_p$ that is used for the $\Delta C'_p$-optimization function. For postflight display purposes, raw $\Delta C'_p$ is passed through the moving-average filter, and the result is called *smoothed* $\Delta C'_p$. Smoothed $\Delta C'_p$ is calculated postflight and only used for display purposes; it is the filtered $\Delta C'_p$ that is the input to the real-time onboard controller.

Although not completely successful, development of the $\Delta C'_p$ measurement system was designed to reduce scatter in the flight data. Calibration of the individual pressure transducers was performed using the same microcontroller used to measure $\Delta C'_p$ in flight. The result was a linear fit with a very small standard deviation of 0.002 in. of water. This was 0.1% of the full range of the leading-edge transducer and 0.2% of full range for the midchord transducer. After individual calibration, the transducers were used to build the system to measure $\Delta C'_p$, which involves dividing the leading-edge pressure differential by the midchord differential. This system was also calibrated using a set of pressures that would result in known $\Delta C'_p$ values, and the standard deviation was found to be about 5% over the range of expected values. (For example, pressure combinations in which $\Delta C'_p$ should be -1.0 resulted in standard deviations of about 0.05.) The ground calibrations were done using static pressures, and so it is possible that the sample-to-sample variations seen in flight were in part due to rapidly changing airfoil pressures resulting from aircraft short-period motion.

Table 2 Summary of flight-test objectives and relevant figures

Flight numbers	Test objectives	Relevant figures
2–9	Comparison of $\Delta C'_p$ data with XFOIL prediction	Fig. 11
10–20	Test of $\Delta C'_p$-maintenance function	Figs. 12 and 13
21–27	Test of $\Delta C'_p$-optimization function	Figs. 14–24

During the flights, airspeed and vertical acceleration were recorded. From these data and known aircraft characteristics, the aircraft coefficient of lift could be determined. For most phases of flight, the lift generated by the horizontal tail and fuselage was assumed to be much less than that generated by the wing, and so the aircraft coefficient of lift was also assumed to be the wing coefficient of lift. Since the planform of the Spirit 100 wing is roughly elliptical, it was further assumed that the airfoil section coefficient of lift at the pressure ports was the same as the wing coefficient of lift. With these assumptions, instantaneous C_l values could be calculated. These values were used with $\Delta C'_p$ values to compare experimental results with XFOIL [12] predictions for the wing airfoil.

Three sets of test flights were completed, each with a different objective. Table 2 provides a summary of the objectives for each set of flights, as well as the numbers of the figures that accompany the analysis of each set. Flight no. 1 is not included in the summary or discussed further because it was merely a shakedown flight to ensure that all of the flight systems worked together.

Comparison of $\Delta C'_p$ Data with XFOIL Prediction

The first set of flights was performed without any controller functions enabled and was intended to collect $\Delta C'_p$ data that could be compared with XFOIL predictions. Flights 2, 3, 4, and 7 contained significant periods of time when the flap was undeflected. The C_L and raw $\Delta C'_p$ values were collected for these periods of time. Figure 11 shows the zero-flap $\Delta C'_p$ data that were obtained from these flights, as well as the XFOIL prediction of $\Delta C'_p$ for a flap angle of 0 deg. Individual $\Delta C'_p$ values are shown with gray × marks, and mean C_L values are shown with black dots. Mean C_L values were determined by grouping raw $\Delta C'_p$ values from -3.5 to 0 into 35 bands, each with a height of 0.1 $\Delta C'_p$. The C_L values in each band were averaged, and so each black dot shows the mean C_L for the $\Delta C'_p$ band in which it lies. Displaying mean C_L values in this manner makes it easy to visually compare experimental results with the XFOIL prediction. (Some of the $\Delta C'_p$ values were artificially recorded as 0 due to the method used to save data; these values are not displayed and were not used to determine mean C_L values.)

For C_L values up to about 1.0, experimental mean C_L values match the XFOIL prediction well. Between C_L values of 1.0 and 1.1, the XFOIL prediction shows a sharp drop in $\Delta C'_p$. This sudden drop is caused by the laminar-to-turbulent boundary-layer transition on the upper surface of the airfoil. The midchord pressure port used to determine $\Delta C'_p$ is located at the 40% chord location. At C_L values below 1.0, XFOIL determines that the boundary layer has not yet transitioned at 40% chord, and so the flow over the pressure port is

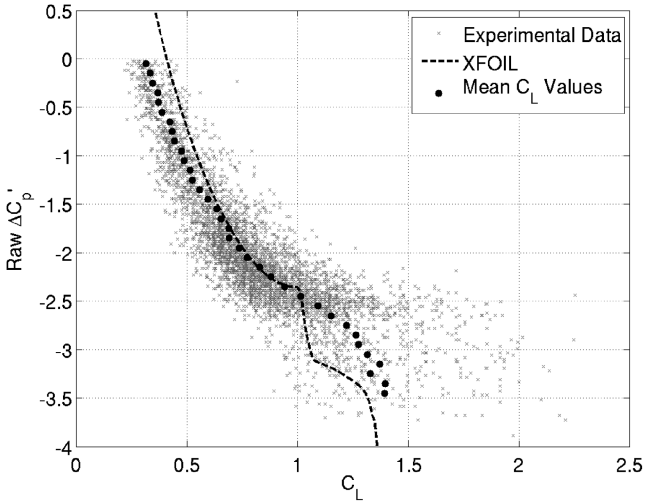

Fig. 11 Comparison of zero-flap raw $\Delta C_p'$ data with XFOIL prediction for flights 2, 3, 4, and 7.

always laminar and the prediction of $\Delta C_p'$ is smooth. At C_L values above 1.1, XFOIL determines that the boundary layer has already transitioned at 40% chord, and so the flow over the port is always turbulent and the $\Delta C_p'$ prediction is again smooth. For C_L values from 1.0 to 1.1, the flow at 40% chord is transitioning from laminar to turbulent, and the upper-surface suction at the pressure port drops rapidly in this range. This is what causes the corners in the XFOIL prediction at C_L values of 1.0 and 1.1. Experimental mean C_L values also show a dropoff in $\Delta C_p'$, but it is less abrupt and occurs at a slightly higher value of C_L. The lack of a sharp corner in the experimental data is to be expected, since transition in flight will be subject to more variability than when it is determined by XFOIL (where the location of transition is always the same for the same input variables).

Test of $\Delta C_p'$-Maintenance Function

The next set of test flights was performed with a controller that implemented the $\Delta C_p'$-maintenance function but not the $\Delta C_p'$-optimization function. The $\Delta C_p'$-maintenance function converts a pilot elevator request into a combination of flap and elevator that provides the desired change in trim lift coefficient, but without any change in trim $\Delta C_p'$. For the Spirit 100 with the manufacturer-specified center of gravity, a request for 1 deg of elevator change is converted into 0.202 deg of elevator and −2.65 deg of flap. This conversion can be seen in Fig. 12, which shows the pilot elevator commands for flight 17 as well as the elevator and flap commands that were generated by the controller and sent to the servos. The top half of the figure shows that the controller reduces the requested elevator deflection to 20.2% of its value, and the bottom half shows that the flap receives −265% of the requested elevator deflection. The signal from the controller is always constrained by the physical limits of the control surface, and this is visible from about 38 to 42 s on the flap graph. The flap limit of 28 deg is reached when the magnitude of the requested elevator deflection reaches approximately 11 deg (28 deg/2.65). For requested elevator deflections above this amount, the controller limits its flap output to 28 deg.

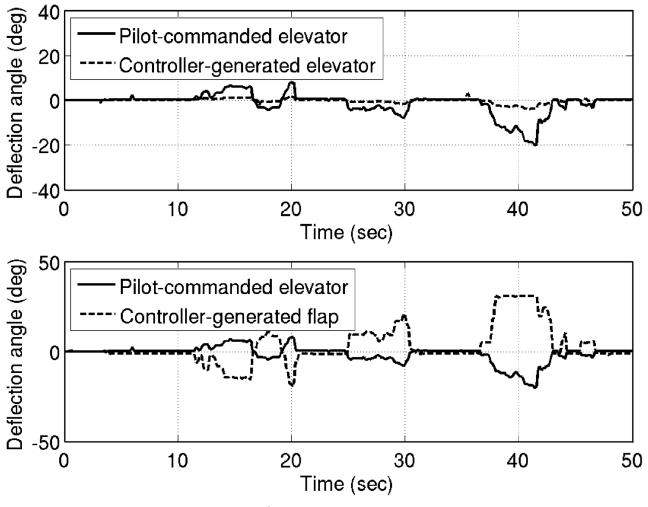

Fig. 12 Results of $\Delta C_p'$-maintenance function for flight 17.

To determine the effectiveness of the $\Delta C_p'$-maintenance function, it is necessary to compare the effect of elevator on $\Delta C_p'$ for the uncontrolled and controlled cases. This is complicated by the fact that $\Delta C_p'$ is affected by lift coefficient, which changes even in the absence of elevator input. Ideally, it should be possible to compensate for this effect. If there are long periods of time over a number of flights in which the flap angle is constant and the controller is disabled, the C_L and $\Delta C_p'$ values can be captured for those times. They can be plotted as they were in Fig. 11, and a least-squares fit can determine the effect of C_L on $\Delta C_p'$. This effect can be subtracted from the actual $\Delta C_p'$ values, both for flights with the controller disabled and flights with the controller enabled, and the difference can be analyzed to determine the effectiveness of the $\Delta C_p'$-maintenance function.

In reality, $\Delta C_p'$ values obtained from experimental flights have a large amount of variation. The experimental mean C_L values in Fig. 11 provide validation of the general shape and trends of the expected curve, but it would be difficult to use them to determine the expected $\Delta C_p'$ for a given measured value of C_L. A specific example of this problem is shown in Fig. 13. The $\Delta C_p'$ data from 19 to 21 s of flight 16 are circled. During this time the elevator and flap were held constant. It is clear that $\Delta C_p'$ values vary greatly within a very small range of C_L values. Regardless of what kind of least-squares fit is used to determine the overall relationship between C_L and $\Delta C_p'$, it would be very difficult, for example, to determine the expected value of $\Delta C_p'$ for a C_L value of 0.35. Near this C_L value there are data points for which measured $\Delta C_p'$ was −0.5 and other data points for which measured $\Delta C_p'$ was −2.4. These data correspond to a flight condition in which the controller is disabled, flap and elevator are constant, and C_L is essentially constant, but there is still considerable movement in $\Delta C_p'$. If $\Delta C_p'$ varies so much under conditions in which it should be essentially constant, it will be very difficult to determine $\Delta C_p'$ differences created by enabling the controller. Since these differences could not be separated from the differences that occur when $\Delta C_p'$ should be essentially constant, it was not possible to determine the effectiveness of the $\Delta C_p'$-maintenance function of the controller.

The inability to verify $\Delta C_p'$-maintenance functionality indicates that analysis of gust-alleviation testing may be particularly difficult. The $\Delta C_p'$-maintenance analysis was performed using smoothed

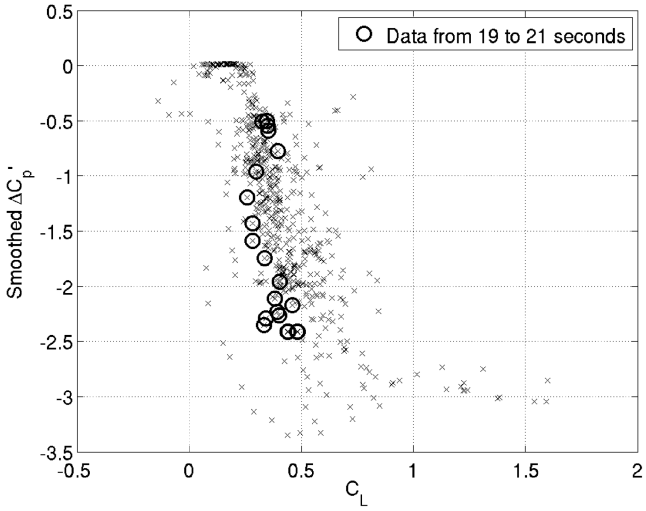

Fig. 13 Flight 16 C_L and $\Delta C_p'$ data highlighting data points from 19 to 21 s.

$\Delta C'_p$, which is obtained by passing raw $\Delta C'_p$ values through a 1 s (10-sample) moving-average filter. The raw $\Delta C'_p$ values have much more sample-to-sample variation than the smoothed values, and the causes of the variations are not known. It is most likely due to a combination of unsteady aerodynamic effects, noise in the system, and other factors not fully understood. Whatever the reason, smoothing of the data is not appropriate for the gust-alleviation function. Some other combination of techniques will be required to reduce the sample-to-sample variations in raw $\Delta C'_p$ data.

Test of $\Delta C'_p$-Optimization Function

The final set of test flights was performed with a controller that implemented both the $\Delta C'_p$-maintenance and $\Delta C'_p$-optimization functions. The aircraft was launched with a high-start launching system that pulled it to altitude before dropping off and allowing the aircraft to begin its glide. As the aircraft is being readied for launch, raw $\Delta C'_p$ values will be zero, since there is no leading-edge pressure differential, and this differential is the numerator of the expression for $\Delta C'_p$. (The denominator, which is the midchord differential, should also be zero but is artificially held at a small value to prevent division-by-zero errors.) Given the amount of time needed to prepare the aircraft for each launch, the filtered $\Delta C'_p$ error goes to 1.85 (which is the raw $\Delta C'_p$ value of 0 minus the target value of -1.85). As the aircraft is pulled aloft by the high start, raw $\Delta C'_p$ becomes negative, and the filtered $\Delta C'_p$ error starts to decrease from 1.85. At the time the aircraft reaches it maximum launch altitude and drops the line from the high start, though, the filtered $\Delta C'_p$ error is still at a high value. At the start of a typical glide, the filtered $\Delta C'_p$ is approximately -0.5, meaning that the filtered $\Delta C'_p$ error is near 1.35. For $\Delta C'_p$ optimization, the goal is to reduce the filtered $\Delta C'_p$ error to zero, which always means that filtered $\Delta C'_p$ goes to the target value of -1.85.

Flight 21 was the first flight with both the $\Delta C'_p$-maintenance and $\Delta C'_p$-optimization functions enabled, and so activation of the controller was delayed until the filtered $\Delta C'_p$ decreased to a value near the target of -1.85. Figure 14 shows the smoothed, filtered, and target $\Delta C'_p$ values for the flight. The time period over which the controller was enabled is shown with a thicker line. At the beginning of the glide, $\Delta C'_p$ was approximately -1.0, and controller activation was delayed until $\Delta C'_p$ was -1.5. This meant that the controller engaged with a fairly small $\Delta C'_p$ error of about $+0.35$. In the figure it is clear that $\Delta C'_p$ continues decreasing until it reaches the target value of -1.85 and then flattens out and oscillates around that value with very small amplitude. Once the controller is disabled for landing at about 62 s, $\Delta C'_p$ drops to about -2 and remains there for the rest of the flight. This figure provides fairly strong evidence that the $\Delta C'_p$-optimization function is effective at keeping filtered $\Delta C'_p$ near the target value of -1.85.

Figure 14 shows large oscillations in smoothed $\Delta C'_p$, and so the data were analyzed using a fast Fourier transform. This technique indicated strong frequency content from 0.1 to 0.2 Hz. This content is similar to that present in the airspeed data, and there is a moderate correlation between variations in $\Delta C'_p$ and airspeed. The displayed oscillations occur in part because changing airspeed affects the measured $\Delta C'_p$. The controller responds to filtered $\Delta C'_p$ and not smoothed $\Delta C'_p$, and so these large oscillations were not even visible to the controller as it attempted to maintain a closed-loop filtered $\Delta C'_p$ value of -1.85. For this flight, the open-loop filtered $\Delta C'_p$ was about -2, since this was the value that was maintained after the controller was disabled at 62 s. This -2 value is not intrinsic to the aircraft, but rather to the trim airspeed. On different flights with different trim airspeeds (due to different pilot-selected elevator trim values), the open-loop filtered $\Delta C'_p$ will be different.

For the time period from 12 to 20 s, Fig. 15 shows the elevator inputs commanded by the pilot and the controller-generated elevator and flap values that are sent to the control surface servos. The controller uses two inputs to generate its output commands. Elevator commands from the pilot are used by the $\Delta C'_p$-maintenance function, and filtered $\Delta C'_p$ error is used by the $\Delta C'_p$-optimization function. The effect of $\Delta C'_p$-maintenance is most clearly visible in the time period from about 14 to 18 s. The pilot generates something similar to a double pulse on the elevator, with the first pulse dropping to about -6 deg and the second pulse dropping to about -7 deg. The $\Delta C'_p$-maintenance function changes this input into an elevator output 20.2% of that requested and a flap output that is -265% of the requested elevator input.

To determine the portion of the controller output that is due to the $\Delta C'_p$-optimization function, the portion due to $\Delta C'_p$ maintenance is subtracted from the final output. The remainder is the optimizing flap, and it is shown in Fig. 16 along with filtered $\Delta C'_p$ error. Flap values are not shown for periods when the controller is disabled, since there is no optimization occurring during these periods.

The spikes that are visible in the plot of optimizing-flap values generally occur when the pilot makes a significant change in elevator position. They are present, in part, because of the small delay between the controller sensing a pilot-generated elevator input and the corresponding output of the $\Delta C'_p$-maintenance function. Although they make the data look noisier than they should be, they do not affect the analysis. One of these spikes results in an optimizing-flap data point less than -20 deg. Although it is included in the analysis, it is cropped out of Fig. 16 to prevent the more important data closer to 0 deg from being visually minimized.

If the data spikes in Fig. 16 are ignored, there is a rough correlation between filtered $\Delta C'_p$ error and optimizing-flap values. As $\Delta C'_p$ error decreases, the optimizing-flap value tends to increase, and vice versa. To better analyze this relationship, optimizing-flap values are plotted

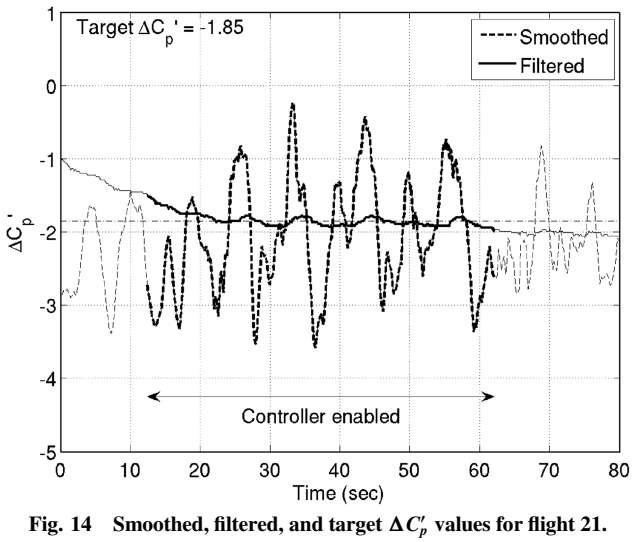

Fig. 14 Smoothed, filtered, and target $\Delta C'_p$ values for flight 21.

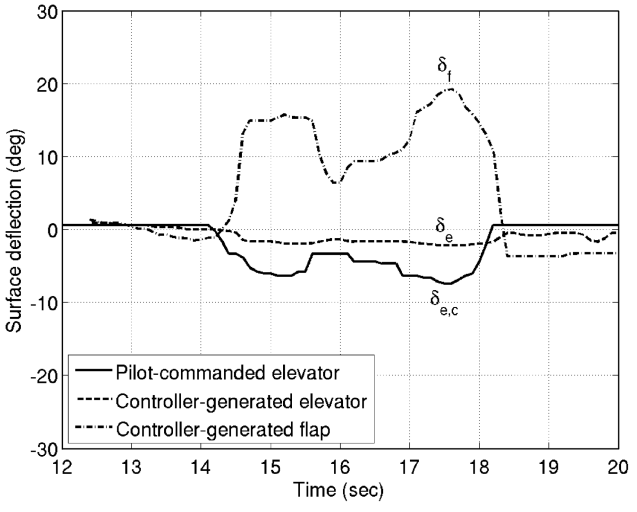

Fig. 15 Pilot-commanded and controller-generated surface deflections for flight 21.

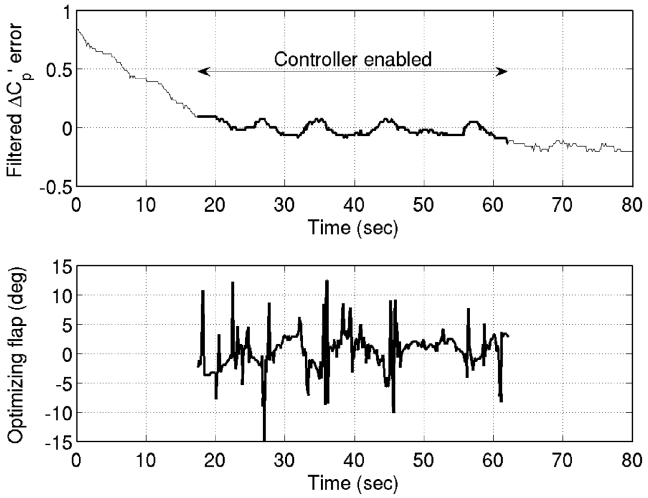

Fig. 16 Filtered $\Delta C_p'$ error and optimizing flap for flight 21.

against filtered $\Delta C_p'$ error values in Fig. 17. For reasons of clarity, displayed optimizing-flap values are cropped to the range from -10 to 10 deg, but all data points are used for the analysis. The displayed filtered $\Delta C_p'$ error values are not continuous, but occur at intervals of about 0.023. This is due to a limitation of the hardware used to record data for postflight analysis. Although the precision of recorded $\Delta C_p'$ values is limited to about two decimal points, the onboard controller had access to $\Delta C_p'$ values with much greater precision.

The relationship between filtered $\Delta C_p'$ error and optimizing flap should be linear, because the controller calculated the flap value using a linear discrete-time state space model. In Fig. 17, the discretization of filtered $\Delta C_p'$ error and the large spread of optimizing-flap values make the expected linear relationship difficult to visualize. For this reason, the mean value of optimizing flap for each discrete filtered $\Delta C_p'$ error was calculated using a scheme in which outlying flap values were given less weight than values closer to the median. These weighted mean flap values are displayed as black dots and make the linear relationship easier to see. A linear least-squares fit of all data was performed, and the resulting line and equation are displayed.

The linear fit indicates that a unit change in filtered $\Delta C_p'$ error results in an optimizing-flap change of approximately -32 deg. To determine if the $\Delta C_p'$-optimization function is modulating the flap properly, this ratio can be compared with the ratio that was programmed into the onboard controller. In flight, filtered $\Delta C_p'$ error is passed through a PI controller with gains $K_P = 4$ and $K_I = 0.195$. When analyzing the slope of a linear fit of experimental results, it is the K_P term that is important. The K_I term will affect the tightness of the fit but will not significantly affect the slope.

Previous analysis of XFOIL $\Delta C_p'$ data and AVL stability derivatives for the Spirit 100 determined the flap change required to achieve a unit change in $\Delta C_p'$ while keeping wing lift constant. This parameter was found to be approximately 9 deg. Adding this much positive flap will cause $\Delta C_p'$ to increase by 1.0. To eliminate a $\Delta C_p'$ error of 1.0 (i.e., to decrease $\Delta C_p'$ from -0.85 to -1.85) would require a flap change of -9 deg, and so it is the negative of the parameter that is used in the controller.

The product of K_P and -9 deg is the constant by which the controller will multiply the filtered $\Delta C_p'$ error in order to generate the optimizing-flap angle. The input (filtered $\Delta C_p'$ error) is multiplied by K_P in the PI controller and then by -9 deg before being output to the servos. The product of K_P and -9 deg is -36 deg, and this is the amount of flap change that should be produced for a unit change in filtered $\Delta C_p'$ error. The linear fit from Fig. 17 has a slope of -32 deg, which is very close to the expected value. This indicates that the controller is implementing the $\Delta C_p'$-optimization algorithm correctly.

Since the controller performed so well on flight 21 with a small starting $\Delta C_p'$ error, it was decided on flight 22 to enable the controller while the error was still large. Figure 18 shows the $\Delta C_p'$ data for this flight. The controller was enabled when the filtered $\Delta C_p'$ was still about -0.65, for an error of 1.20. The $\Delta C_p'$-optimization function handles this larger starting error well, with the filtered $\Delta C_p'$ dropping below the target value and then steadily rising back up. This dip below the -1.85 target is caused by the small integral term K_I in the PI controller. When the controller is engaged with a large positive error, the integral portion of the controller state continues to increase as the error drops toward zero. When the error gets to zero at about 15 s, the integral portion of the controller state is positive and proportional to the area under the error curve (and above the target line of -1.85). To zero-out this area, the integral term K_I actuates the flap to drive the error negative, and the running mean value of the error will stay negative until there is as much area above the error curve as there is below.

After the successful controller performance in flights 21 and 22, the next flight was flown with the controller disabled. It was necessary to demonstrate that the close tracking of $\Delta C_p'$ was due to the controller and that the aircraft would not maintain a $\Delta C_p'$ close to the target -1.85 value on its own. Figure 19 shows the $\Delta C_p'$ values for the uncontrolled flight 23. It is clear that the aircraft did not track the target $\Delta C_p'$ and that the close tracking observed in flights 21 and 22 must have be due to the controller, as expected.

Flights 21 through 23 were performed at normal airspeeds for the Spirit 100, around 9–10 m/s. Flight 24 was flown with the controller disabled at a higher airspeed, around 12–16 m/s This was done to

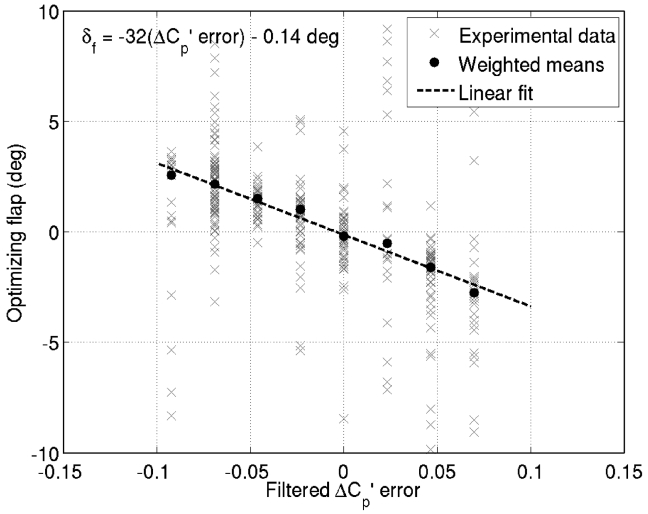

Fig. 17 Least-squares fit of filtered $\Delta C_p'$ error and optimizing flap for flight 21.

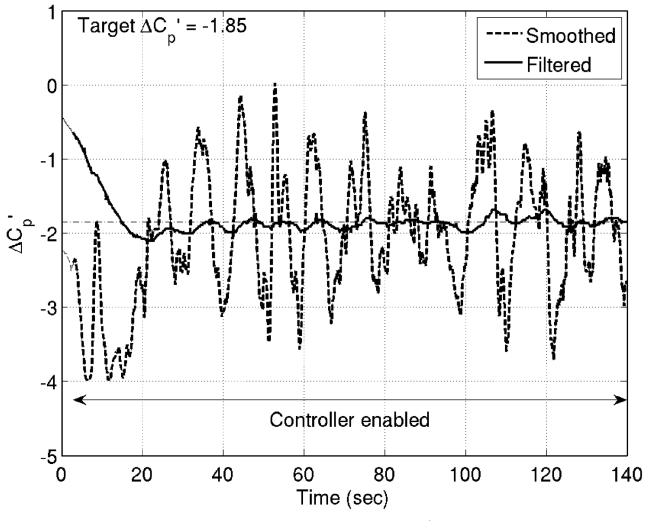

Fig. 18 Smoothed, filtered, and target $\Delta C_p'$ values for flight 22.

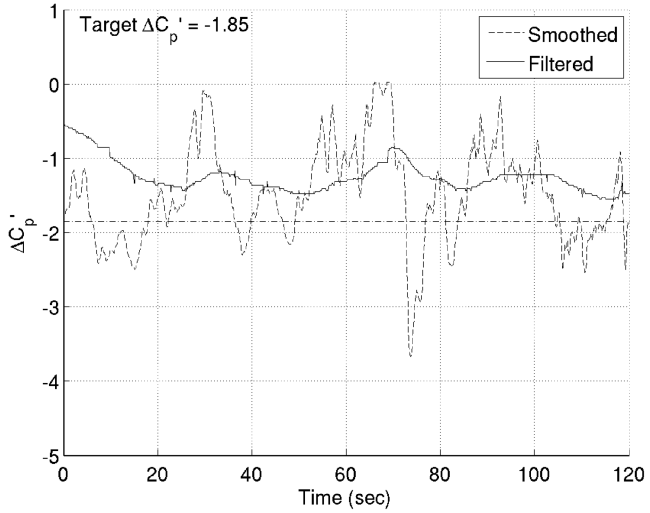

Fig. 19 Smoothed, filtered, and target $\Delta C'_p$ values for flight 23.

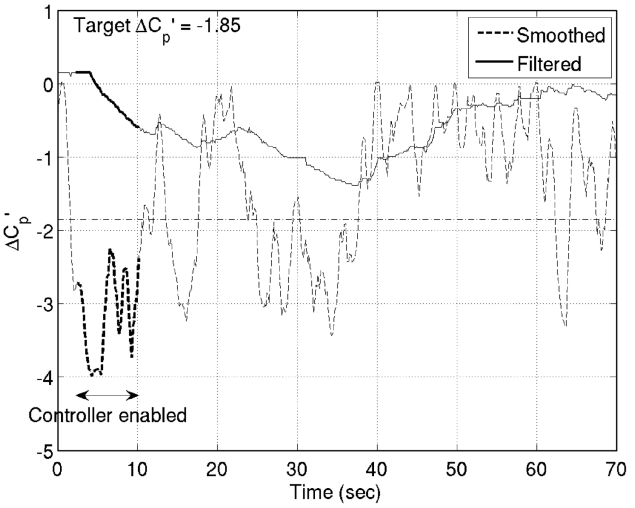

Fig. 21 Smoothed, filtered, and target $\Delta C'_p$ values for flight 25.

generate $\Delta C'_p$ values that were much higher than those on previous flights. Figure 20 shows that this was accomplished, with filtered $\Delta C'_p$ error values that reached and maintained the maximum recordable value of 2.0 (corresponding to a filtered $\Delta C'_p$ value of 0.15). Because of the manner in which $\Delta C'_p$ values were recorded for postflight analysis, error values greater than 2.0 were recorded as 2.0. It is almost certain that the $\Delta C'_p$ errors displayed in Fig. 20 as 2.0 were even higher in flight. (This limit on recorded values did not apply to the $\Delta C'_p$ values that were used in flight by the controller; it had access to any actual $\Delta C'_p$ error values that exceeded 2.0. Thus, nonlinearity due to controller input saturation was not an issue.)

For flight 25, the high-start launch was flown with a high airspeed, and the controller was enabled very shortly after the high start disconnected and the glide portion of the flight began. The value of $\Delta C'_p$ was still very high at this point, as can be seen in Fig. 21. Filtered $\Delta C'_p$ is still constrained at 0.15 when the controller was enabled, and from the slope of the curve it is likely that its value was probably closer to 0.7 (for an error of 2.25). Within a few seconds the pilot commented that he felt he did not have control of the aircraft. He attempted some more elevator commands but felt that the aircraft was not responding to his input. About 8 s after the controller had been enabled, the pilot disabled it and control of the aircraft was regained. The aircraft was then landed with the controller disabled.

The aircraft was thoroughly checked to ensure that the loss of control had not been due to aircraft damage or looseness of mechanical or electrical connections. Even before this flight, however, it had been known that enabling the controller with a very high filtered $\Delta C'_p$ error could cause a problem. The source of the problem is the ratio of flap and elevator movement required for $\Delta C'_p$ optimization and the ratio of maximum flap and elevator throws.

From the center (0 deg) position, the half-range of flap throw (to either full up or full down) was approximately 28 deg. The half-range of elevator throw was approximately 23.5 deg. If the integral term of the PI controller is ignored, about -36 deg of flap is required to correct a unit of filtered $\Delta C'_p$ error, as determined previously. This is about 129% of the available half-range of flap throw. For the elevator, about -12 deg is required, or about 51% of available throw. If the filtered $\Delta C'_p$ error was 1.0 when the controller was enabled, the elevator would deflect to its calculated value of -12 deg. The flap would need to deflect to -36 deg to offset the pitching moment of the elevator, but would be constrained to its half-range of -28 deg. Effectively, this would be an uncommanded flap deflection of $+8$ deg and would result in the pilot no longer having full control of the aircraft. This issue was evident whenever the controller was enabled on the ground as part of the preflight checks. With a $\Delta C'_p$ of zero (with no flow over the wings) and a filtered $\Delta C'_p$ error of $+1.85$, both flap and elevator angles would start decreasing as soon as the controller was enabled. The flaps would reach their limit within a few seconds, and the elevator would continue to decrease to its limit while the flaps were constrained at theirs. The fact that either control surface reached its limit before the other indicated that there were flight conditions under which there could be a loss of control.

Postflight analysis of the data indicated that this was what had caused the problem, as shown in Fig. 22. The controller was enabled

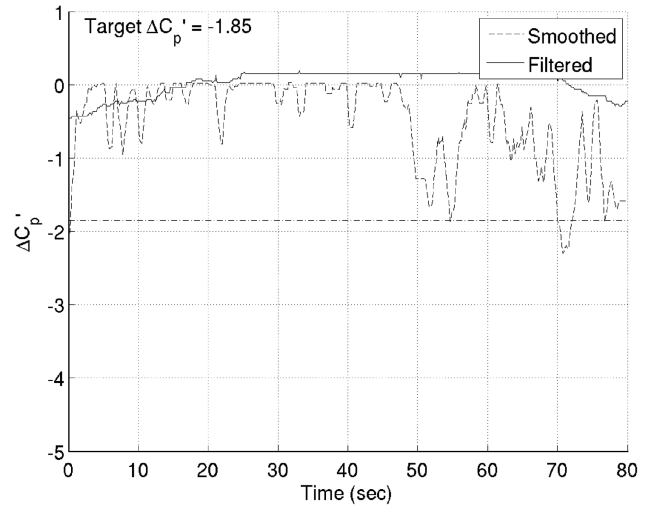

Fig. 20 Smoothed, filtered, and target $\Delta C'_p$ values for flight 24.

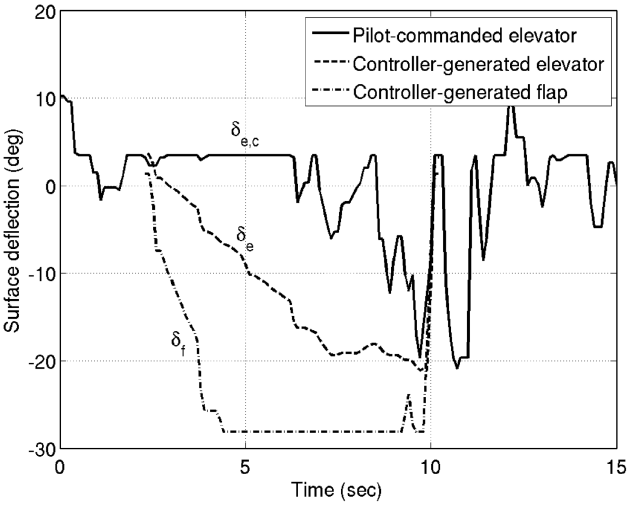

Fig. 22 Pilot-commanded and controller-generated surface deflections for flight 25.

at about 2 s, and about 2 s later the flap saturated at its lower limit. Until this occurred, the aircraft was under control and responded appropriately. When the flap saturated, the elevator angle was about −6 deg, and it continued to decrease an additional 15 deg without a corresponding decrease in flap angle. About 2 s after saturation, the pilot saw that the aircraft was not responding appropriately and began entering elevator commands. If those elevator commands had been passed directly to the elevator, they would likely have been sufficient to regain control. But the controller was enabled, and $\Delta C'_p$ maintenance reduced the elevator response to 20.2% of the commanded input. Normally, the missing 79.8% of elevator response would be compensated for by moving the flap −265% of the requested elevator input, and the combination of 20.2% elevator and −265% flap would give the pilot the aircraft response that is desired. But in this case, the flap was saturated and could not move, and so the aircraft response was only 20.2% of what the pilot expected. This furthered the (correct) pilot belief that he did not have control of the aircraft. After about 4 s of elevator commands, the pilot disabled the controller. The flap returned to its original value near center and future stick inputs were passed unmodified to the elevator. This allowed the pilot to regain control and terminate the flight.

Ignoring the integral term of the PI controller, $\Delta C'_p$ optimization will cause saturation of the flap to occur whenever filtered $\Delta C'_p$ is greater than −1.1 (meaning filtered $\Delta C'_p$ error is greater than about 0.75). There is one caveat to this statement. When the controller is first enabled, the $\Delta C'_p$-optimization portion of the output is not immediately applied, but is ramped up linearly over a period of about 5 s. This is to prevent a step input from being sent to the flap and elevator servos. If filtered $\Delta C'_p$ is greater than −1.1 when the controller is enabled, but less than this value at the end of the ramp period, the flap may not saturate. This is what occurred at the beginning of the earlier flight 22, for which $\Delta C'_p$ values were previously shown in Fig. 18. When the controller was enabled at 3 s, the value of filtered $\Delta C'_p$ was about −0.65, well above the saturation limit of −1.1. But the ramp function means that very little of the $\Delta C'_p$-optimization response is passed to the servos immediately after the controller is enabled. In flight 22, the full response was not passed to the servos until about 8 s, and filtered $\Delta C'_p$ had fallen to −1.2 by then. The ramp function may have been intended to prevent large step inputs from being passed to the servos, but it had the additional benefit of preventing flap saturation in cases like this in which $\Delta C'_p$ is high but falling when the controller is enabled.

After a discussion regarding the likely cause of the loss of control in flight 25, the pilot felt more comfortable about leaving the controller enabled even if the controls felt sluggish shortly after it was enabled. The $\Delta C'_p$ data for flight 26 are shown in Fig. 23. The controller was enabled with a large positive filtered $\Delta C'_p$ error, and there was saturation of the flap. Although this temporarily resulted in reduced control of the aircraft, the pilot left the controller enabled,

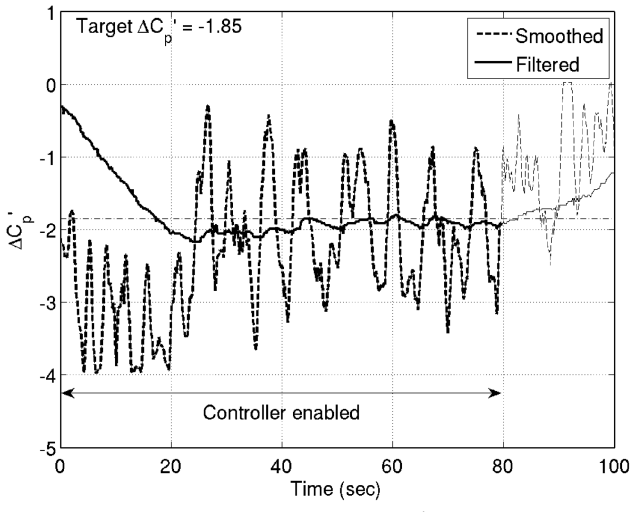

Fig. 23 Smoothed, filtered, and target $\Delta C'_p$ values for flight 26.

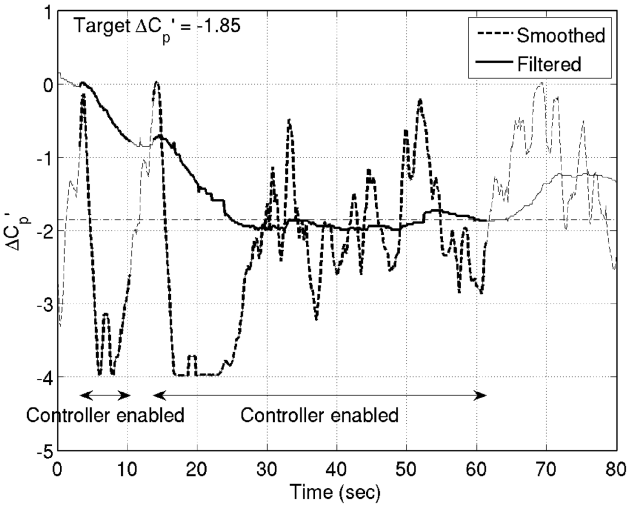

Fig. 24 Smoothed, filtered, and target $\Delta C'_p$ values for flight 27.

because it was understood that this would occur. After about 5 s, $\Delta C'_p$ fell to the point that saturation ceased, and full control of the aircraft was regained.

Flight 27 was the final test flight, and its $\Delta C'_p$ data are shown in Fig. 24. The controller was enabled with a large filtered $\Delta C'_p$ value of almost 0, and saturation quickly occurred. This resulted in a stall and rapid loss of altitude, and so the controller was disabled after about 7 s. Within a few seconds the aircraft had recovered, and the controller was reenabled. By the end of the second ramp period, $\Delta C'_p$ had dropped to about −1.2, and so saturation did not occur again. The remainder of the flight was uneventful.

Flights 21 through 27 clearly showed the effectiveness of the $\Delta C'_p$-optimization function. When the controller was enabled, filtered $\Delta C'_p$ moved immediately toward the target value of −1.85, and it showed no tendency to do so with the controller disabled. The effect of the proportional term in the PI controller was calculated and determined to be very close to the value that was expected based on the programming of the controller. The effect of the small integral term was apparent by observing the slow correction in filtered $\Delta C'_p$ after an initial overshoot.

Conclusions

This research attempted to show the effectiveness of the $\Delta C'_p$-optimization and $\Delta C'_p$-maintenance functions that were previously demonstrated in simulations. The $\Delta C'_p$-optimization function was shown to be effective, since the filtered $\Delta C'_p$ error was driven toward zero whenever the controller was enabled. This occurred under various aircraft conditions of speed and lift coefficient. Passing the $\Delta C'_p$ error through a low-pass filter removed transients and provided the $\Delta C'_p$-optimization function with a relatively smooth signal.

Evaluation of the $\Delta C'_p$-maintenance function used unfiltered $\Delta C'_p$ values that were found to contain large sample-to-sample variations. This high-frequency content could not be explained in terms of changing coefficient-of-lift values. Demonstration of the effectiveness of $\Delta C'_p$ maintenance required the ability to accurately predict $\Delta C'_p$ values based on known lift coefficients and flap angles. The variations made these predictions impossible, and so $\Delta C'_p$-maintenance effectiveness could not be proven.

The gust-alleviation function that was demonstrated in simulations was not attempted for these flight tests. The rapid servo response required for gust alleviation can be achieved in simulations by modeling servos as continuous-time components with very small time constants. The R/C servos used in this flight testing, however, were discrete-time components with responses that would not have been sufficient for gust alleviation. Flight testing of this function may require more expensive servos with much better response times, or possibly specialized analog servos (which operate as continuous-time components).

Even with more capable servos, the gust-alleviation function may be very difficult to test on aircraft of the size that was used for this research. A gust that would cause a moderate $\Delta C'_p$ change in a general aviation aircraft would cause an extremely large change in an R/C-sized aircraft such as the Spirit 100. Additionally, the small time constants associated with smaller aircraft place greater demands on the control system, the operation of which is already affected by the large sample-to-sample variations in $\Delta C'_p$.

For at least some NLF airfoils, the optimal $\Delta C'_p$ for drag minimization is a constant (independent of flap deflection, angle of attack, and lift coefficient). This is not the case for the low-Reynolds-number SD7037 airfoil used on the Spirit 100. The controller developed in this research maintained a constant target $\Delta C'_p$ that reduced drag over a subrange of the expected lift coefficients. Future controllers could minimize drag over a larger range of lift coefficients by holding constant some nonlinear function of flap deflection and $\Delta C'_p$. Alternatively, the function could be replaced with a lookup table of optimal flap and $\Delta C'_p$ values.

The raw $\Delta C'_p$ values that were recorded showed variations that seemed unusually large. The aircraft used for this research was relatively small, and the most important step in advancing this research would be to implement $\Delta C'_p$ measurement on a much larger aircraft. Larger R/C aircraft may give better results, but, ideally, the $\Delta C'_p$-measuring technique used in this research should be implemented on full-sized manned aircraft. The longer time constants of these larger aircraft would make it easier to determine if the $\Delta C'_p$ variations were the result of noise or actually indicative of rapidly varying pressures on the wing. Manned aircraft can also be flown at altitudes at which freestream turbulence can be much less than that common at altitudes at which R/C aircraft are flown.

Acknowledgments

The authors would like to acknowledge KalScott Engineering for their partial support of this research through a Phase-2 Small Business Technology Transfer Program project from the NASA Dryden Research Center. Partial support for the first author was also provided by the Frank C. Ziglar Jr. Endowed Graduate Fellowship and is gratefully acknowledged. Pilotage and support were provided by the flight-test team, which consisted of Stearns Heinzen, Adam Propst, Dave Burke, and Jason Bishop. Permission by Great Planes Model Manufacturing Company to use the copyrighted illustration of the Spirit 100 sailplane is gratefully acknowledged.

References

[1] Pfenninger, W., "Investigation on Reductions of Friction on Wings, in Particular by Means of Boundary Layer Suction," NACA TM 1181, Aug. 1947.

[2] Pfenninger, W., "Experiments on a Laminar Suction Airfoil of 17 Per Cent Thickness," *Journal of the Aeronautical Sciences*, Vol. 16, No. 4, April 1949, pp. 227–236.

[3] McGhee, R. J., Viken, J. K., Pfenninger, W., Beasley, W. D., and Harvey, W. D., "Experimental Results for a Flapped Natural-Laminar-Flow Airfoil with High Lift/Drag Ratio," NASA TM 85788, May 1984.

[4] Somers, D. M., "Design and Experimental Results for a Flapped Natural-Laminar-Flow Airfoil for General Aviation Applications," NASA TP 1865, June 1981.

[5] Drela, M., "Elements of Airfoil Design Methodology," *Applied Computational Aerodynamics*, Vol. 125, edited by P. A. Henne, AIAA, Washington, D.C., 1990, pp. 167–189.

[6] McAvoy, C. W., and Gopalarathnam, A., "Automated Cruise Flap for Airfoil Drag Reduction over a Large Lift Range," *Journal of Aircraft*, Vol. 39, No. 6, Nov.–Dec. 2002, pp. 981–988. doi:10.2514/2.3051

[7] Vosburg, V., and Gopalarathnam, A., "The Stability and Control of an Aircraft with an Adaptive Wing," AIAA Paper 2004–4814, Aug. 2004.

[8] Cox, C., Hall, C. E., Jr., and Gopalarathnam, A., "Analysis of Different Stabilizing Control Systems for Aircraft with Automated Cruise Flaps," AIAA Paper 2006–6134, Aug. 2006.

[9] Cox, C., Hall, C. E., Jr., and Gopalarathnam, A., "Development of Stable Automated Cruise Flap for an Aircraft with Adaptive Wing," *Journal of Aircraft*, Vol. 46, No. 1, Jan.–Feb. 2009, pp. 301–311. doi:10.2514/1.38684

[10] *Spirit 100 Almost-Ready-to-Fly Instruction Manual*, Great Planes Model Manufacturing Co., Champaign, IL, 2005.

[11] Drela, M., and Youngren, H., *AVL 3.26 User Primer*, Dept. of Aeronautics and Astronautics, Massachusetts Inst. of Technology, Cambridge, MA, April 2006, http://web.mit.edu/drela/Public/web/avl/ [retrieved 3 Dec. 2009].

[12] Drela, M., "XFOIL: An Analysis and Design System for Low Reynolds Number Airfoils," *Low Reynolds Number Aerodynamics*, edited by T. J. Mueller, Lecture Notes in Engineering, Vol. 54, Springer–Verlag, New York, June 1989, pp. 1–12.

[13] Cox, C. A., "Development and Flight Test of a Multi-Function Controller for Automated Cruise Flaps on an Aircraft Wing," Ph.D. Thesis, North Carolina State Univ., Raleigh, NC, Dec. 2008.